Journal of ELECTRONIC MATERIALS, Vol. 48, No. 9, 2019
https://doi.org/10.1007/s11664-019-07147-0

$Cu(Zn,Sn)(S,Se)_2$ Solar Cells with a Nanocomposite Window Layer Produced by Totally Nonvacuum Methods

THỊ THU HIEN NGUYEN,[1,4] ANH TUAN PHAM,[4] DUC HUY TRAN,[2] VIET ANH DUNG DANG,[3] NGOC PHAN VU,[1] HUU DUNG NGUYEN,[1] THANH TUNG DUONG,[1] and DUY CUONG NGUYEN[1,5]

1.—Nano Optoelectronics Laboratory, Advanced Institute for Science and Technology, Hanoi University of Science and Technology, No. 1 Dai Co Viet, Hai Ba Trung, Hanoi, Vietnam. 2.—School of Materials Science and Engineering, Hanoi University of Science and Technology, No. 1 Dai Co Viet, Hai Ba Trung, Hanoi, Vietnam. 3.—School of Chemical Engineering, Hanoi University of Science and Technology, No. 1 Dai Co Viet, Hai Ba Trung, Hanoi, Vietnam. 4.—Faculty of Power System, Electric Power University, 235 Hoang Quoc Viet Str, Tu Liem Dist, Hanoi, Vietnam. 5.—e-mail: cuong.nguyenduy@hust.edu.vn

The authors report the optical and electrical properties of nanocomposite films of Ag-nanowires (Ag-NWs) and indium-tin oxide nanoparticles (ITO-NPs) and their application in window electrodes in solar cells. We found that the electrical and optical properties of Ag-NWs/ITO-NPs nanocomposite films strongly depend on the thickness. Nanocomposite film with 1000 nm thickness was observed to be most suitable for application as window electrodes in $Cu(Zn,Sn)(S,Se)_2$ solar cells. The parameters of the cell using a 1000 nm-thick nanocomposite window electrode are short-circuit current density of 24.2 mA/cm^2, open-circuit voltage of 0.32 V, fill factor of 0.44, and conversion efficiency of 3.37%. The results demonstrated an economical pathway for fabricating solar cells without vacuum methods.

Key words: CZTSSe solar cells, nanocomposite, Ag nanowire, ITO nanoparticles, nonvacuum methods

INTRODUCTION

Compound solar cells made from $Cu(Zn,Sn)(S,Se)_2$ (CZTSSe) have received much attention from researchers around the world because of their attractive properties, such as high stability, inexpensive starting materials, and routine fabrication methods.[1–4] In addition, the band gap of the CZTSSe material, which varies from 1.0 eV to 1.5 eV, is suitable for achieving high solar conversion efficiency. The physical properties of these materials are easily controlled by varying the ratio of Se/Se or Zn/Sn.[5] Because their starting materials are environmentally friendly and relatively inexpensive, CZTSSe solar cells are promising candidates for replacing conventional thin solar cells, such as CdTe and $Cu(In,Ga)Se_2$ (CIGS). The CZTSSe absorber layer in CZTSSe solar cells can be fabricated via either vacuum or nonvacuum techniques, such as sputtering, evaporation, spray pyrolysis or printing.[6–9] Interestingly, CZTSSe cells fabricated by simple nonvacuum methods show a higher conversion efficiency than those made by vacuum methods. In the literature, the best conversion efficiency of CZTSSe solar cells is 12.6% by a nonvacuum method, and 11.6% by a vacuum method.[10,11] To reduce the cost of solar cells, the fabrication process should be simple, fast, and cheap. Hence, nonvacuum methods are more advantageous than vacuum-based methods. While CZTSSe absorber layers have been fabricated by many researchers using nonvacuum methods, the window layers in these solar cells, such as ZnO and Indium tin oxide (ITO) or Al-doped ZnO, were still

(Received September 18, 2018; accepted March 14, 2019; published online April 1, 2019)

deposited by vacuum methods.[12–15] Some research groups have fabricated transparent conductive oxide (TCO) films by nonvacuum methods.[16,17] However, during the fabrication process of TCO films, they must be annealed at high temperatures to enhance electrical properties. Hence, this approach is not applicable for the fabrication of window electrodes in the chalcopyrite solar cells like CIGS and CZTSSe, because it will affect the CdS buffer layer.

In this research, we aim to fabricate CZTSSe solar cells using only nonvacuum methods. The ITO window layer is prepared from ITO nanoparticles in combination with Ag-nanowire (Ag-NW). This study examines the effect of Ag-NW/ITO-NP nanocomposite window layers on the photovoltaic properties of CZTSSe solar cells. The optical, electrical, and photovoltaic properties of the nanocomposite window layer, as well as cell devices, are investigated thoroughly.

EXPERIMENTAL

Materials

CZTS nanoparticles were synthesized at 225°C under ambient nitrogen using the hot-injection method. The details of the CZTS nanoparticle synthesis process were shown in a previous report.[18] Cu (II) acetylacetonate (Tokyo Chemical Industry), zinc acetylacetonate (Tokyo Chemical Industry), tin(IV) bis(acetylacetonate) dibromide (97% purity, Aldrich), and sulfur powder (99% purity, Kishida) were used as starting materials. Oleylamine was used as the solvent. The atomic ratio of Cu:In:Sn:S the precursor was 1:0.69:0.56:3; and the atomic ratio of the elements in the obtained CZTS nanoparticles is $Cu_1(Zn_{0.68}, Sn_{0.52})S_{1.88}$. After synthesis, the CZTS nanoparticles were washed, dried, and subsequently dispersed in hexanethiol to form a stable CZTS nanoparticle ink.

For the preparation of ITO nanoparticle ink, 0.02 g of polyvinyl alcohol (PVA) was dissolved in 0.4 ml of distilled water. In this instance, PVA acts as the adhesion material. Subsequently, iso-propanol (4 ml) was slowly injected into the PVA/water mixture to obtain a transparent solution. The process was carried out carefully to avoid rapid injection, which may cause a precipitate of PVA in the solution, resulting in poor ITO films after coating. After iso-propanol mixing, 0.4 g of ITO nanoparticles (Aldrich), each with a diameter of $\sim$30 nm, were added to form ITO ink for making the window layer. All steps for preparing the ITO ink were performed under magnetic stirring.

Device Fabrication

The CZTSSe device consists of Ag (electrodes), ITO-NPs, Ag-NWs, CdS, CZTSSe, a Mo/glass substrate. At first, CZTS films were printed on the Mo/glass substrate by the doctor-blade method using CZTS nanoparticle ink under ambient air. The CZTS film thickness varies between 0.7 μm and 1 μm. After printing, these porous CZTS films were annealed at 520°C under ambient Se vapor for 20 min to obtain highly dense CZTSSe films. Next, a 50-nm CdS buffer layer was deposited on the CZTSSe films by the chemical bath deposition (CBD) method. For preparing the window layers, Ag-NW and then ITO-NP layers were deposited by the doctor-blade method. The Ag-NW solution was obtained by dispersing Ag-NWs with a diameter of $\sim$ 130 nm (purchased from Seashell Technologies) in isopropyl alcohol. The Ag-NW layer was printed onto the CdS layer, then dried at 100°C for several minutes. Afterwards, ITO nanoparticles were coated onto the Ag-NW layer, and subsequently dried at 100°C for 2 min. It should be emphasized that the coating of the ITO-NPs on the Ag-NWs was carried out very gently because the adhesion between the Ag-NWs and the CdS layer was very poor. The overall thickness of the Ag-NW/ITO-NP window layer was controlled by the number of ITO printing steps while the Ag-NWs were printed only once. Finally, cells with an area of 0.5×0.5 cm^2 were separated by mechanical scribing, then attached to an Ag electrode for testing.

Analysis Methods

Surface morphology and film thickness were analyzed by scanning electron microscopy (SEM) (JSM-7600F, Jeol). The composition of the CZTS nanoparticles and CZTSSe films were measured by energy dispersive x-ray spectroscopy (EDS) (JSM-7600F, Jeol) at an accelerating voltage of 10 kV. Phase structure, preferred orientation, and crystallinity of the CZTS nanoparticles and CZTSSe films were investigated by x-ray diffraction (XRD) (D8 Advance, Bruker). The transmittance of the Ag-NW/ITO-NP films was recorded by UV–Vis spectroscopy (Cary 5000 UV–Vis–NIR). Photovoltaic measurements were performed on an AM 1.5 solar simulator equipped with a 450-W xenon lamp. *I–V* curves were obtained by applying an external bias to the cell and measuring the generated photocurrent with a DC voltage current source.

RESULTS AND DISCUSSION

Surface SEM images of Ag-NWs and nanocomposite films with different thicknesses are shown in Fig. 1. Figure 1a shows that the distribution of the Ag nanowires is not uniform. For nanocomposite films, as the film thickness increases, the density of the Ag nanowires seen on the surface of the films decreases significantly. The surface of nanocom-

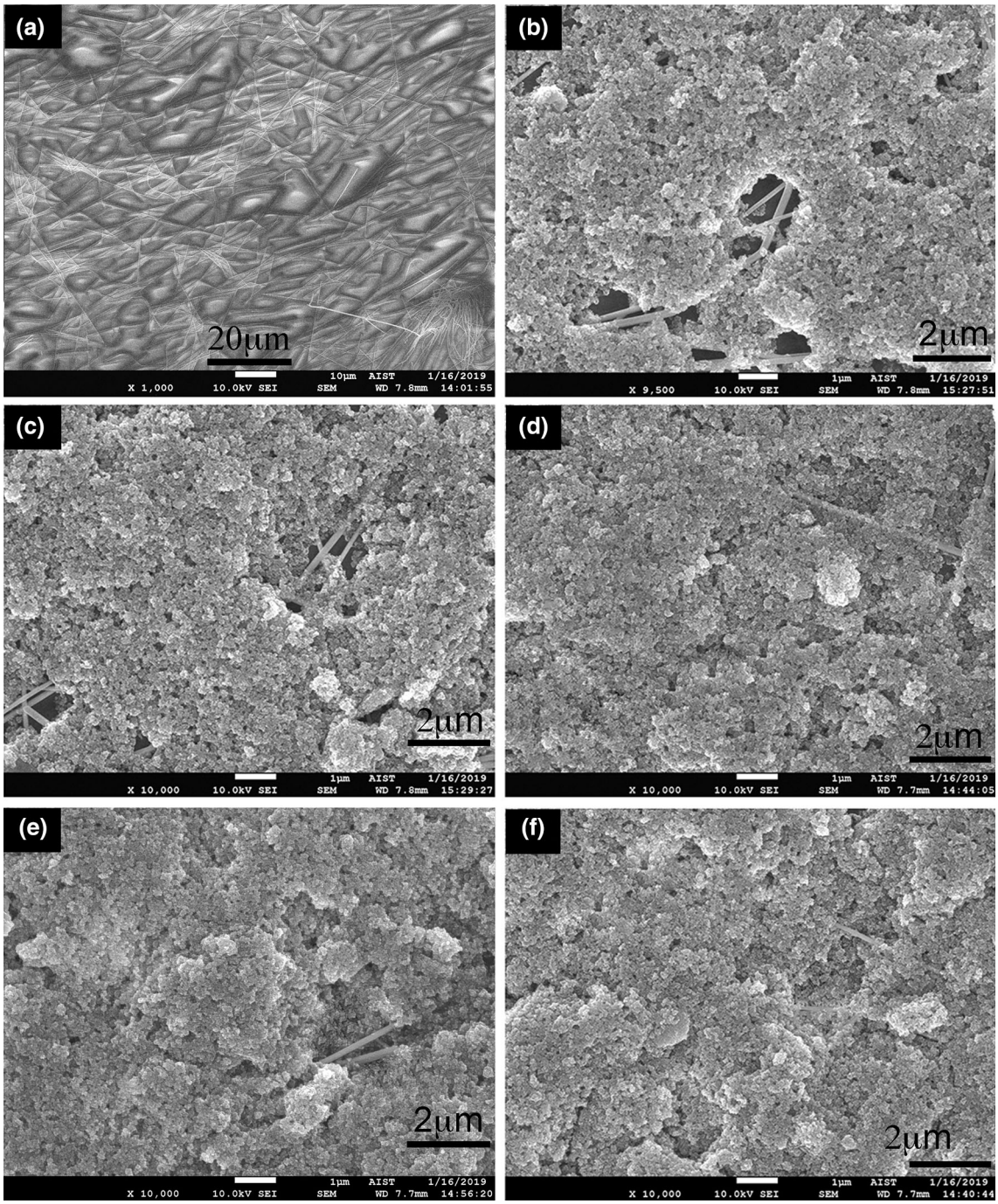

Fig. 1. Surface SEM image of Ag-NW/ITO-NP nanocomposite films with thicknesses of (a) Ag-NWs only, (b) 520 nm, (c) 770 nm, (d) 1000 nm, (e) 1240 nm, and (f) 1760 nm.

posite films is quite rough, and it is difficult to distinguish the difference in roughness between films.

The sheet resistance and resistivity with different film thicknesses are shown in Fig. 2. The sheet resistance value of Ag-NW/ITO-NP nanocomposite films decreased with the increase of film thickness in the range of 520–1240 nm and did not change when the thickness increased from 1240 nm to 1760 nm. The lowest sheet resistance value was observed in a 1240-nm-thick film, at $\sim$ 10.2 Ω/□. These sheet resistance values were close to those of commercial ITO wafers. The resistivity calculated from sheet resistance and film thickness is also shown in Fig. 2. The resistivity values varied in the range of 11.9×10^{-2} to 20×10^{-2} Ω · cm when the thickness of Ag-NW/ITO-NP films increased from 520 nm to 1760 nm. Contrary to the sheet resistance values, the resistivity values increased with

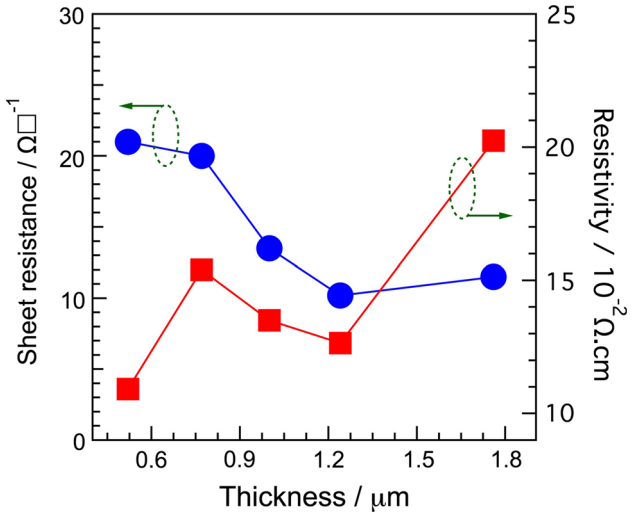

Fig. 2. Variation of sheet resistance and resistivity of Ag-NW/ITO-NP films with thicknesses of 520 nm, 770 nm, 1000 nm, 1240 nm, and 1760 nm.

increasing film thickness. The trends can be explained by the relative contribution between Ag-NWs and ITO layers. Because the Ag-NW layer was printed only once for all samples, the number of Ag-NWs in these films is constant. However, the thicknesses of the films were controlled by the number of ITO-NPs printed, and thus correlated to the number of ITO-NPs. As a result, the resistivity increased with an increasing ITO-NP/Ag-NW ratio and film thickness. To further confirm the trend, we fabricated an ITO-NP film without Ag-NWs. The ITO-only sample had very high sheet resistance, nearly to the point of being an insulator (see supplementary table S1). The sheet resistance values of 1000-nm and 1240-nm films are lower than that of 770-nm film, which may be caused by a nonuniform distribution of Ag-NWs on the sample surface. To test the uniformity of the sheet resistance of Ag-NW/ITO-NP films, we prepared samples of a 2.5×2.5 cm^2 size on glass substrates and found that thick films (> 1000 nm) showed better uniformity than thin films (< 1000 nm) (see supplementary Figure S1 and Table S1).

According to the above results, Ag nanowires, not ITO nanoparticles, are the major conductor of electricity in nanocomposite electrodes. That leads to the question of what causes the sheet resistance of the nanocomposite electrodes to be lower than that of the Ag-NW electrodes. The resistance of Ag nanowire electrodes consists of Ag-NW resistance (denoted R_{AgNWs}) and contact resistance (denoted R_{CONTACT}) between two nanowires, as described in Fig. 3. After mixing with ITO nanoparticles, the junction of two Ag nanowires produces two resistances, R_{CONTACT} (Ag-NW/Ag-NW) and the resistance of Ag-NW/ITO/Ag-NW parallel to each other, as described in Fig. 3. Thus, the contact resistance between wires is reduced, and results in the reduction of the sheet resistance, which may be the reason the sheet resistance of nanocomposite electrodes is lower than that of Ag-NWs alone. Some research groups have also reported on this problem; they used metal or welding techniques to improve the contact resistance between Ag nanowires.[19–21]

The transmittance of the nanocomposite ITO-NP/Ag-NW films with different thicknesses is shown in Fig. 4. In general, the transmittance decreases as the film thickness increases, as expected. The transmittance of the nanocomposite films with thicknesses of 520 nm, 770 nm, 1000 nm, 1241 nm, and 1760 nm at the wavelength of 550 nm were 78.1%, 74.7%, 70.4%, 66.5%, and 63.0%, respectively. The transmittance of all films in the wavelength range of 500–1100 nm was relatively stable and high, which included the strongest wavelength region in the solar spectrum. The results demonstrated the suitability of the nanocomposite films for window electrodes in solar cells. In the infrared region (1100–2000 nm), the transmittance decreased considerably, which can be explained by the free electrons in the ITO nanoparticles. The incident light with a lower frequency than the plasma frequency of the ITO nanoparticles is reflected, thus causing a decrease in transmission. The relationship between plasma frequency and free electron concentration is described in Eq. 1 below:

$$\omega_p^2 = \frac{ne^2}{m^* \varepsilon_o}, \tag{1}$$

where ω_p is the plasma frequency, n is the free electron density, m^* is the effective mass of an electron, ε_o is the vacuum dielectric constant, and e is the charge of an electron. TCO materials typically have a plasma frequency in the infrared region, so the transmittance of these materials in this region is significantly reduced by reflection. As a result, the light transmittance of low-sheet resistance films is limited because the diameter of Ag nanowires is large, and the nanocomposite films are too thick. It is our guess, that to overcome the limitation of the transmittance, it is necessary to reduce the thickness of nanocomposite films by using Ag nanowires and ITO nanoparticles with smaller diameters.

Figure 5 shows the XRD pattern of CZTS films on Mo/glass substrates before and after annealing under ambient Se vapor at 520°C for 20 min. Diffraction peaks of CZTS film without annealing are observed at 28.41°, 47.35°, and 56.19°. These peaks correspond to the preferred orientations of CZTS (112), CZTS(220), and CZTS(312), respectively.[22] No second phase was observed in the CZTS films without annealing. This indicates that the nanoparticles used for printing the films were single phase CZTS. In addition, the peak intensity was rather weak, indicating low crystallinity of CZTS film without annealing. For the annealed film, the diffraction peaks are viewed at 2θ angles of 27.36°,

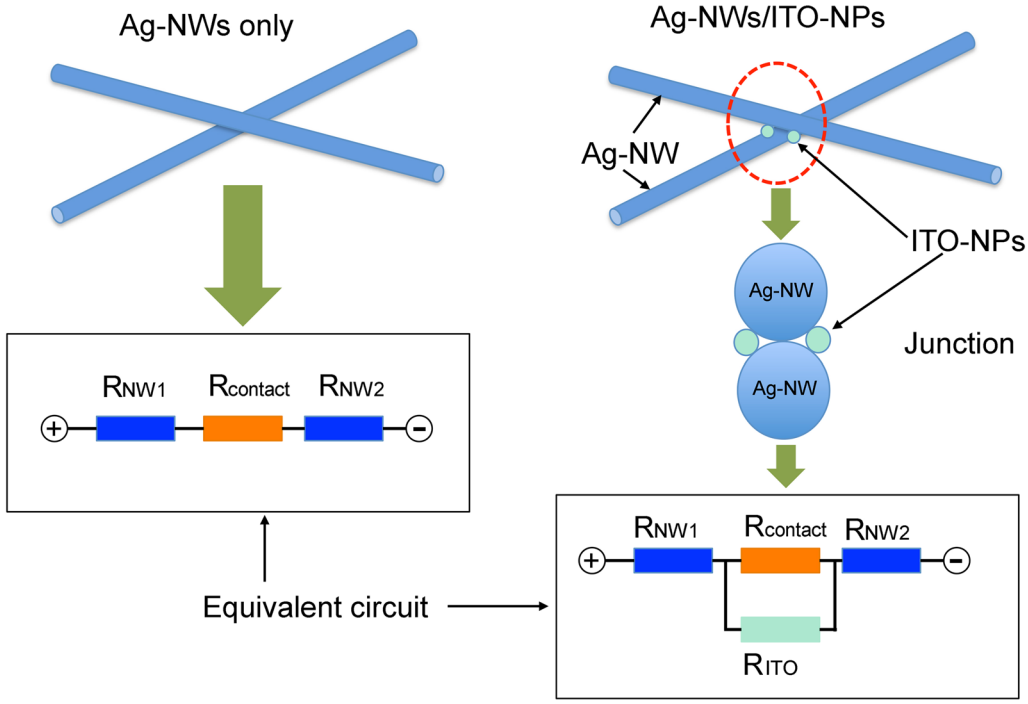

Fig. 3. Illustration of Ag-NWs only and Ag-NW/ITO-NP composite films.

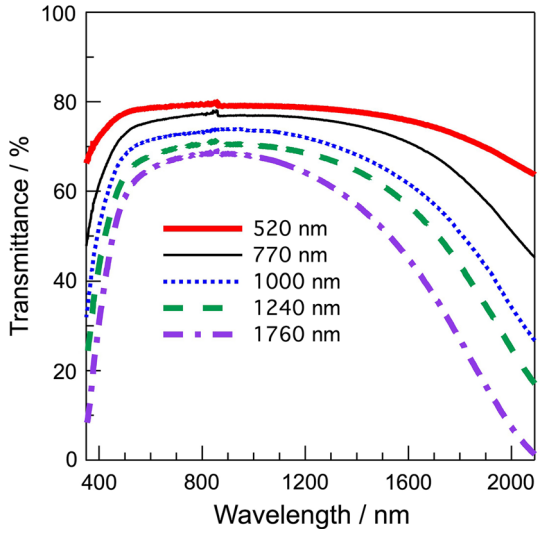

Fig. 4. Transmittance spectra of Ag-NW/ITO-NP films with thicknesses of 520 nm, 770 nm, 1000 nm, 1240 nm, and 1760 nm.

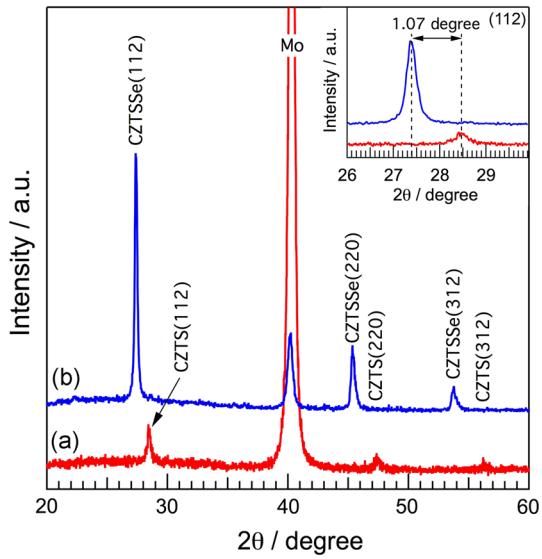

Fig. 5. XRD pattern of CZTS films on Mo substrates (a) before and (b) after annealing under ambient Se vapor at 520°C for 20 min. The inset shows (112) XRD peaks of CZTS before and after selenization.

45.36°, and 53.76°, which are indexed as the preferred orientation of CZTSSe(112), CZTSSe(220), and CZTSSe(312), respectively. After annealing under ambient Se vapor, only single phase CZTSSe exists in the films. The intensity of diffraction peaks was very strong, indicating a high crystallinity. As shown in the inset of Fig. 5, a peak shift towards a smaller angle was observed after annealing. This shift is due to the replacement of sulfur ions by selenium ions during annealing. The larger radius of the Se^{2-} ion (198 pm) in comparison with the S^{2-} ion (184 pm) caused a peak shift towards the lower angle.[23,24]

Figure 6 shows an SEM image of the cross-section and surface of the CZTSSe cell. The surface of the devices shows that Ag-NWs were mixed with ITO-NPs to form an Ag-NW/ITO-NPs nanocomposite. The distribution of Ag-NWs is not homogenous. Large particles can be seen on the surface. The appearance of these large particles is caused by the

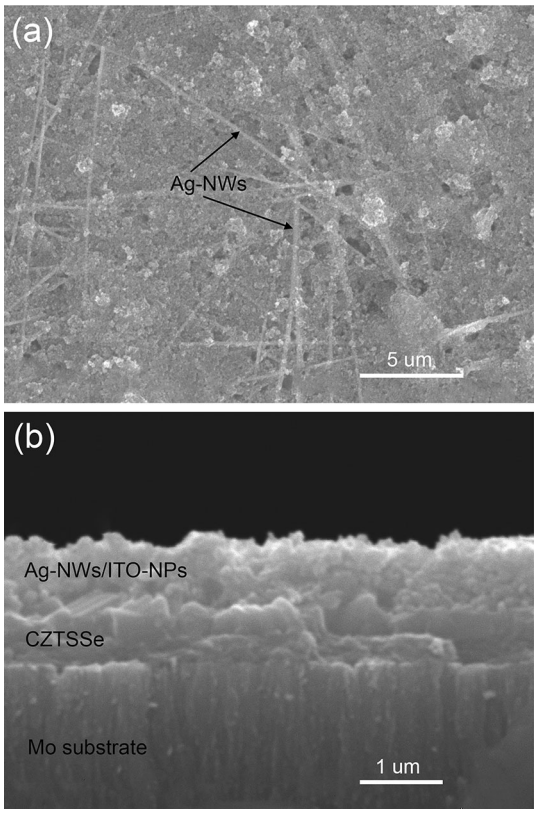

Fig. 6. SEM images of (a) the surface and (b) cross-section of the best CZTSSe cell using a 1000-nm Ag-NW/ITO-NP film for the window layer.

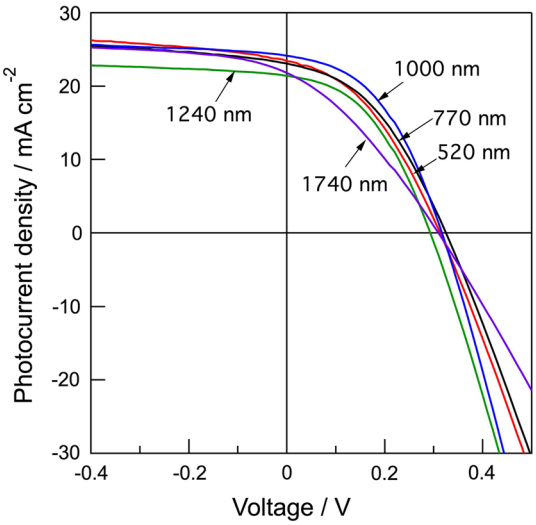

Fig. 7. Photocurrent density–voltage curves of CZTSSe solar cells with different printed Ag-NW/ITO-NP window layer thicknesses.

Table I. Photovoltaic parameters of CZTSSe cells with different Ag/ITO thicknesses

Ag/ITO thickness (nm)	J_{SC} [mA/cm^{-2}]	V_{OC} [V]	FF	Efficiency [%]
520	23.4	0.31	0.39	2.88
770	23.08	0.32	0.41	3.05
1000	24.2	0.32	0.44	3.37
1240	21.4	0.29	0.43	2.69
1780	21.8	0.32	0.32	2.13

poor dispersion of ITO-NPs in the water/isopropanol/PVA solution.

To analyze the effect of Ag-NW/ITO-NP window layers on the photovoltaic properties of CZTS device parameters, we fabricated CZTS cells with different Ag-NW/ITO-NP film thicknesses. The photocurrent density–voltage curves of these cells are shown in Fig. 7, with photovoltaic parameters tabulated in Table I. The cells with thick Ag-NW/ITO-NP layers, 1240 nm and 1760 nm, show a poor photovoltaic property. This can be related to the low transmittance of 1240 nm and 1760 nm Ag-NW/ITO-NP layers, as shown in Fig. 4. The best cell performance was observed in a 1000-nm Ag-NW/ITO-NP film, with photovoltaic parameters of short-circuit current density (J_{SC})=24.2 mA/cm^2, open-circuit voltage (V_{OC})=0.32 V, fill factor (FF)=0.44, and conversion efficiency (η)=3.37%. Based on photovoltaic characteristics, it can be concluded that a 1000-nm nanocomposite film with a sheet resistance of 13.5 Ω/□ and transmittance of ~70% is the most suitable for making the window electrode in CZTSSe solar cells.

Compared with our previous studies using ITO films fabricated by sputtering,[18] the typical parameters of solar cells using nanocomposite window electrodes are lower, which may be due to nanocomposite films having a lower transmittance than sputtered-ITO films. However, the advantages of Ag-NW/ITO-NP nanocomposite films are that they can be fabricated under air pressure and room temperature conditions, so it does not affect the buffer layer in the chalcopyrite solar cells. In addition, equipment used for synthesizing nanocomposite films is simple and inexpensive.

CONCLUSIONS

We fabricated CZTSSe solar cells using nonvacuum methods only. The sheet resistance of the Ag-NW/ITO-NP nanocomposite films is relatively low, varying in the range of ~10 to 21 Ω/□, which is appropriate for window layers in compound solar cells. A high transmittance of nanocomposite films was observed at wavelengths in the range of 500–1100 nm, implying that these films are appropriate for window electrodes. The optimal cell was achieved at a 1000-nm-thick Ag-NW/ITO-NP layer. The obtained parameters of this cell included a J_{SC}

of 24.2 mA/cm^2 and a conversion efficiency of 3.37%. The results demonstrated an economical pathway to fabricating solar cells without using vacuum methods.

ACKNOWLEDGMENTS

This research is funded by the Vietnam National Foundation for Science and Technology Development (NAFOSTED) under Grant Number 103.02-2017.45.

ELECTRONIC SUPPLEMENTARY MATERIAL

The online version of this article (https://doi.org/10.1007/s11664-019-07147-0) contains supplementary material, which is available to authorized users.

REFERENCES

1. K. Tanaka, M. Oonuki, N. Moritake, and H. Uchiki, *Sol. Energy Mater. Sol. Cells* 93, 583 (2009).
2. Q. Guo, G.M. Ford, W.C. Yang, B.C. Walker, E.A. Stach, H. W. Hillhouse, and R. Agrawal, *J. Am. Chem. Soc.* 132, 17384 (2010).
3. G. Larramona, S. Bourdais, A. Jacob, C. Chone, T. Muto, Y. Cuccaro, B. Delatouche, C. Moisan, D. Pere, and G. Dennler, *J. Phys. Chem. Lett.* 5, 3763 (2014).
4. T.K. Todorov, J. Tang, S. Bag, O. Gunawan, T. Gokmen, Y. Zhu, and D.B. Mitzi, *Adv. Energy Mater.* 3, 34 (2013).
5. S. Chen, X.G. Gong, A. Walsh, and S.-H. Wei, *Appl. Phys. Lett.* 94, 041903 (2009).
6. Y.P. Lin, T.E. Hsieh, Y.C. Chen, and K.P. Huang, *Sol. Energy Mater. Sol. Cells* 162, 55 (2017).
7. J.K. Kim, S.H. Park, S.W. Ryu, J.H. Oh, and B.H. Shin, *Prog. Photovolt. Res. Appl.* 25, 308 (2017).
8. ThH Nguyen, W. Septina, S. Fujikawa, F. Jiang, T. Harada, and S. Ikeda, *RSC Adv.* 5, 77565 (2015).
9. X. Lin, J. Kavalakkatt, M.Ch. Lux-Steiner, and A. Ennaoui, *Adv. Sci.* 2, 1500028 (2015).
10. W. Wang, M.T. Winkler, O. Gunawan, T. Gokmen, T.K. Todorov, Y. Zhu, and D.B. Mitzi, *Adv. Energy Mater.* 4, 1301465 (2014).
11. I. Repins, C. Beall, N. Vora, C. DeHart, D. Kuciauskas, P. Dippo, B. To, J. Mann, W.C. Hsu, A. Goodrich, and R. Noufi, *Sol. Energy Mater. Sol. Cells* 101, 154 (2012).
12. T.K. Todorov, K.B. Reuter, and D.B. Mitzi, *Adv. Energy Mater.* 22, 156 (2010).
13. C. Steinhagen, M.G. Panthani, V. Akhavan, B. Goodfellow, B. Koo, and B.A. Korgel, *J. Am. Chem. Soc.* 131, 12554 (2009).
14. K. Woo, Y. Kim, and J. Moon, *Energy Environ. Sci.* 5, 5340 (2012).
15. W. Yang, H.S. Duan, B. Bob, H. Zhou, B. Lei, C.H. Chung, S. H. Li, W.W. Hou, and Y. Yang, *Adv. Mater.* 24, 6323 (2012).
16. K.E. Lee, M.S. Wang, E.J. Kim, and S.H. Hahn, *Curr. Appl. Phys.* 9, 683 (2009).
17. Z. Chen, W. Li, R. Li, Y. Zhang, G. Xu, and H. Cheng, *Langmuir* 29, 13836 (2013).
18. D.C. Nguyen, S. Ito, and D.V.A. Dung, *J. Alloys Compd.* 632, 676 (2015).
19. E.C. Garnett, W. Cai, J.J. Cha, F. Mahmood, S.T. Connor, M.G. Christoforo, Y. Cui, M.D. McGehee, and M.L. Brongersma, *Nat. Mater.* 11, 241 (2012).
20. L. Hu, H.S. Kim, J.Y. Lee, P. Peumans, and Y. Cui, *ACS Nano* 4, 2955 (2010).
21. H. Lu, D. Zhang, X. Ren, J. Liu, and W.C.H. Choy, *ACS Nano* 8, 10980 (2014).
22. Joint committee for powder diffraction standards, No.26-0575, *Mater. Res. Bull.* 9, 645 (1974).
23. H.W. Lehmann and M. Robbins, *J. Appl. Phys.* 37, 1389 (1966).
24. Y. Iwadate, K. Kawamura, K. Igarashi, and J. Mochinaga, *J. Phys. Chem.* 86, 5205 (1982).